Supporting Information

Synthesis of $K[B_3H_7NH_2BH_2NH_2B_3H_7]$ for K-ion solid-state electrolyte

Xi-Meng Chen,[a] Si-Han Jia,[a] Jia-Xin Kang,[a] Yichun Zhang,[a] Yubin Ma,[a] Yiming Ma,[a] Xin Jiang,[a] Xing-Chao Yu,[a] Pengtao Qiu,*[a] and Xuenian Chen*[a,b]

[a]*School of Chemistry and Chemical Engineering, Henan Key Laboratory of Boron Chemistry and Advanced Energy Materials, Henan Normal University, Xinxiang, Henan 453007, China*

[b]*College of Chemistry, Zhengzhou University, Zhengzhou, Henan 450001, China*

*E-mails: xuenian_chen@zzu.edu.cn; qiupengtao@htu.edu.cn

1. Experimental section:

1.1. General procedures. All manipulations were carried out on a Schlenk line or in a glove box filled with high-purity nitrogen. The ^{11}B NMR and $^{11}B\{^{1}H\}$ NMR spectra were recorded at 193 MHz spectrometer and externally referenced to $BF_3{\cdot}OEt_2$ in C_6D_6 (δ = 0.00 ppm). The ^{1}H NMR and $^{1}H\{^{11}B\}$ NMR spectra were obtained at 600 MHz spectrometer. IR spectra were measured by a Spectrum 400F. Elemental analyses were carried out on an Elementar (Vario EL) instrument. The thermal behaviours of compounds were determined by synchronous thermal analyses (TGA-DSC and TGA-MS, Netzsch 449 C Jupiter/QMS 403D).

Single-crystal X-ray diffraction analysis of compound was recorded on an Agilent SuperNova Dual diffractometer using graphite monochromated Cu Kα radiation, λ = 1.54184 Å. The crystal data and selected bond distances of $K[B_3H_7NH_2BH_2NH_2B_3H_7]{\cdot}$18-crown-6 were summarized in Tables S1 and S2. Further details on the crystal structure investigation can be obtained free of charge from The Cambridge Crystallographic Data Centre *via* www.ccdc.cam.ac.uk/data_request/cif on quoting the depository number CCDC-2122765.

KH was washed with tetrahydrofuran (THF) and n-hexane and then dried in vacuo. KNH_2BH_3 and $NH_3B_3H_7$ were prepared according to the literature methods.[1,2] All of the solvents were distilled from standard drying agents and degassed before use.

1.2. Synthesis of $K[B_3H_7NH_2BH_2NH_2B_3H_7]$ through the reaction of KH with $NH_3B_3H_7$. $NH_3B_3H_7$ (0.17 g, 3.0 mmol) and KH (0.08 g, 2.0 mmol) were added to a 50 mL Schlenk flask. The flask was connected with a Schlenk line, and 15 mL THF was injected. Then, the reaction solution was stirred at −40 °C for 1 hour (Fig. S1), and a white precipitate was formed (Fig. S2). After filtration, THF was removed from the filtrate under dynamic vacuum to leave a white powder. The residue was washed with CH_2Cl_2 (3 × 20 mL), and then dried under vacuum. 15 mL THF was injected to the flask, and then 2mL n-hexane was dropped into the THF solution until a small amount of white precipitate was appeared. After filtration, THF and n-hexane were removed from the filtrate under dynamic vacuum to leave a white powder product $K[B_3H_7NH_2BH_2NH_2B_3H_7]$ (0.14 g, 86% yield). ^{11}B NMR (193 MHz, CD_3CN): δ −8.55

(*t*, *J* = 103.8 Hz, *B*H_2), −17.11 (*br*, 4 B of 2 *B*H*B* in 2 B_3H_7), −25.48 (*br*, 2 B of 2 *B*H_2 in 2 B_3H_7) ppm (Fig. 1a). $^{11}B\{^1H\}$ NMR (193 MHz, CD_3CN): δ −8.55 (*s*, *B*H_2) , −17.11 (*s*, 4 B of 2 *B*H*B* in 2 B_3H_7), −25.48 (*s*, 2 B of 2 *B*H_2 in 2 B_3H_7) ppm(Fig. 1b).^1H NMR (600 MHz, CD_3CN) δ 2.32 (*br*, 4 H of 2 NH_2), 1.86 (*m*, 2 H of BH_2), 1.05 (*br*, 14 H of 2 B_3H_7) ppm (Fig. S3a). $^1H\{^{11}B\}$ NMR (600 MHz, CD_3CN) δ 2.32 (*br*, 4 H of 2 NH_2), 1.86 (*m*, 2 H of BH_2), 1.06 (*s*, 14 H of 2 B_3H_7) ppm (Fig. S3b). IR (cm^{-1}): 3313 (s), 3270 (s), 2480 (s), 2432 (s), 2279 (m), 2209 (w), 1540 (s), 1380 (w), 1206 (s), 1164 (s), 1116(s), 1053 (s), 949(s), 900(s), 691(w) (Fig. S4). Anal. Calcd for $K[B_3H_7NH_2BH_2NH_2B_3H_7]$: H, 12.37; N, 17.19. Found: H, 12.03; N, 17.35.

1.3. Synthesis of $K[B_3H_7NH_2BH_2NH_2B_3H_7]$ through the reaction of $K[NH_2BH_3]$ with $NH_3B_3H_7$. $NH_3B_3H_7$ (0.17 g, 3.0 mmol) and $K[NH_2BH_3]$ (0.14 g, 2.0 mmol) were added to a 50 mL Schlenk flask. The flask was connected with a Schlenk line and 15 mL THF was injected. The reaction solution was stirred at room temperature for 24 hours (Fig. S15), and a white precipitate was formed (Fig. S16 and S17). After filtration, THF was removed from the filtrate under dynamic vacuum to leave a white powder. The residue was washed with CH_2Cl_2 (3 × 20 mL), and then dried under vacuum to yield a white powder product $K[B_3H_7NH_2BH_2NH_2B_3H_7]$ (0.12 g, 74% yield). ^{11}B NMR (193 MHz, CD_3CN): δ −8.58 (*t*, *J* = 103.8 Hz, *B*H_2), −17.10 (*br*, 4 B of 2 *B*H*B* in 2 B_3H_7), −25.54 (*br*, 2 B of 2 *B*H_2 in 2 B_3H_7) ppm (Fig. S5a). $^{11}B\{^1H\}$ NMR (193 MHz, CD_3CN): δ −8.58 (*s*, *B*H_2), −17.06 (*s*, 4 B of 2 *B*H*B* in 2 B_3H_7), −25.47 (*s*, 2 B of 2 *B*H_2 in 2 B_3H_7) ppm (Fig. S5b).^1H NMR (600 MHz, CD_3CN) δ 2.31 (*br*, 4 H of 2 NH_2), 1.87 (*m*, 2 H of BH_2), 1.08 (*br*, 14 H of 2 B_3H_7) ppm (Fig. S6a). $^1H\{^{11}B\}$ NMR (600 MHz, CD_3CN) δ 2.32 (*br*, 4 H of 2 NH_2), 1.86 (*m*, 2H of BH_2), 1.05 (*s*, 14 H of 2 B_3H_7) ppm (Fig. S6b).

1.4. Electrochemical measurement. Electrochemical impedance spectroscopy (EIS) was used for the ionic conductivity. The as-synthesized compounds were pressed into pellets with 6.35 mm diameter in glove box. And the thickness of the pellets was measured by a calibrated Mitutoyo digital caliper. All EIS measurements utilized a homemade airtight cell, in which stainless use steel (SUS) was used as electrode. The EIS spectra from 1 Hz to 10^5 Hz with a 10 mv AC signal were collected by an Autolab

AUT88031 potentiostat after maintaining the cell for 30 min at a given temperature. Ionic conductivity (σ, S cm^{-1}) was calculated by the equation $\sigma = d/(R \times A)$, where R (Ω), A (cm^{-2}), and d (cm) are electrolyte resistance, effective contact area between electrolyte and electrode, and thickness of the electrolyte, respectively. The activation energies (E_a) were evaluated by Arrhenius equation $\sigma T = A_0 \exp(-E_a/kT)$, where A_0 and k are pre-exponential factor and Boltzmann constant, respectively. Linear sweep voltammetry (LSV) from open circuit voltage (OCV) to 4 V and −0.05 V (vs K^+/K) at a scan rate of 0.1 mV s^{-1} in a K/electrolyte/SUS cell were measured for the electrochemical stability window. The direct current (DC) through the K/electrolyte/K cells in the voltage of 50 mV and the resistances before and after polarization of electrolyte were recorded for the K-ion transference number (t_{K^+}), which was calculated by the equation $t_{K^+} = I_s (\Delta V - I_0 R_0) / I_0 (\Delta V - I_s R_s)$, where ΔV (V), I_0 (A), R_0 (Ω), I_s (A), and R_s (Ω) are DC polarization potential, the initial current, the resistance before polarization, the steady current, and the resistance after polarization, respectively. Galvanostatic cycling data of a K/electrolyte/K cell were recorded at a constant current density of 0.01 mA cm^{-2} with a cycling interval of 1h at 45 °C on a multichannel battery testing system (LAND CT3001A) for the compatibility with K metal.

1.5. Computational details. The geometry optimization was performed Gaussian 09 software at B3LYP-D3(BJ)/6-311G(d,p) level.[3] The structures were obtained from the single-crystal data, and only the position of hydrogen atoms was optimized. The ESP was analyzed by Multiwfn code and rendered by VMD.[4,5]

2. Supporting results:

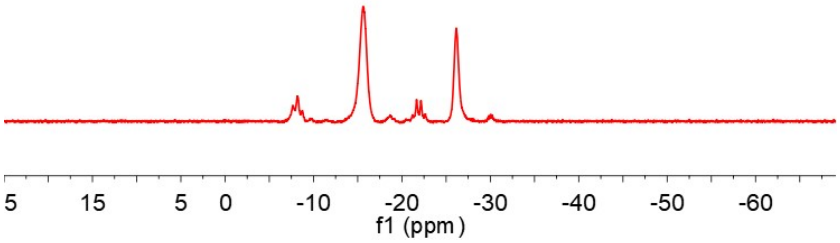

Fig. S1 The ^{11}B NMR spectrum of the reaction solution of KH with $NH_3B_3H_7$ in THF.

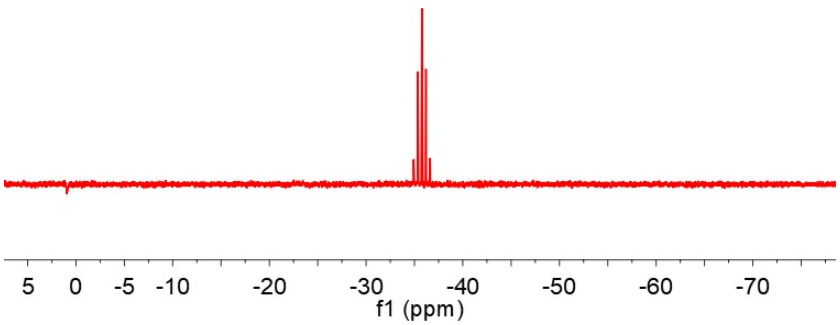

Fig. S2 The ^{11}B NMR spectrum of KBH_4 formed in the reaction of KH with $NH_3B_3H_7$ in DMSO.

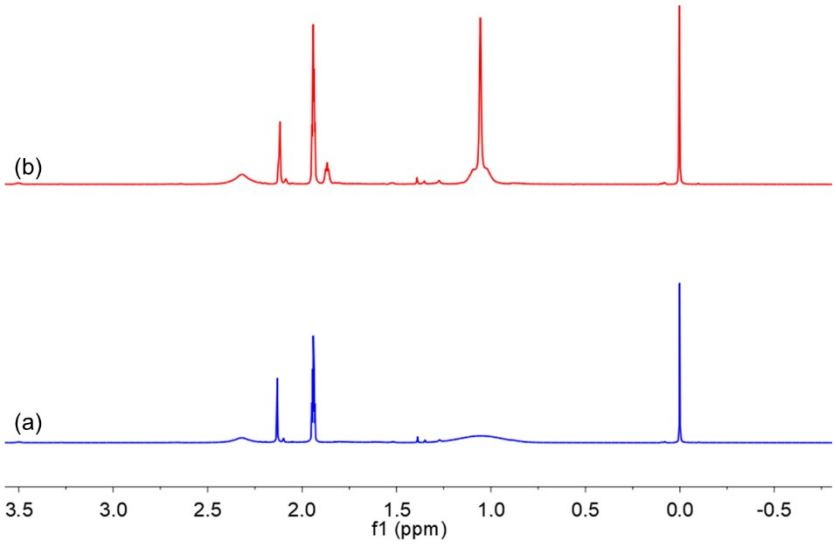

Fig. S3 The ^{1}H NMR (a) and $^{1}H\{^{11}B\}$ NMR (b) spectra of $K[B_3H_7NH_2BH_2NH_2B_3H_7]$ in CD_3CN, which was isolated from the reaction of KH with $NH_3B_3H_7$.

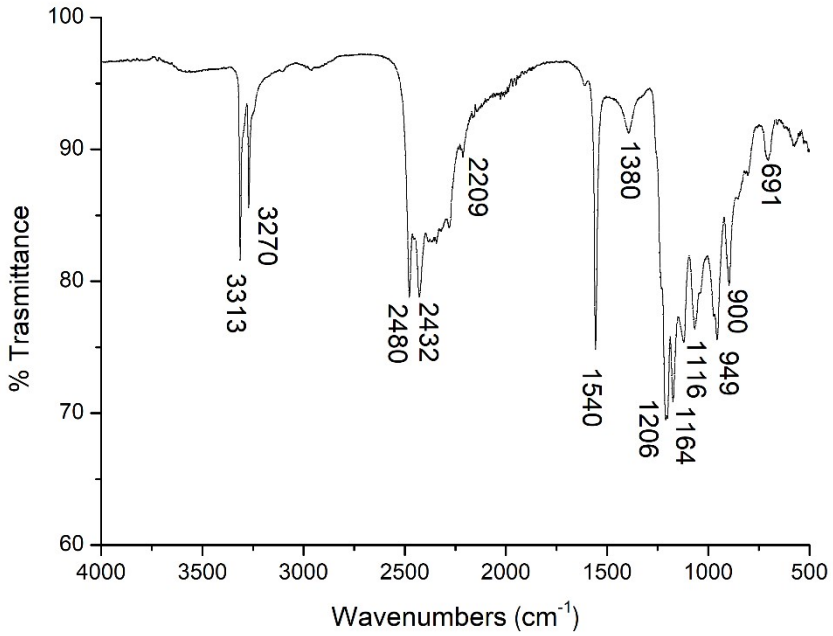

Fig. S4 The IR spectrum of $K[B_3H_7NH_2BH_2NH_2B_3H_7]$, which was isolated from the reaction of KH with $NH_3B_3H_7$.

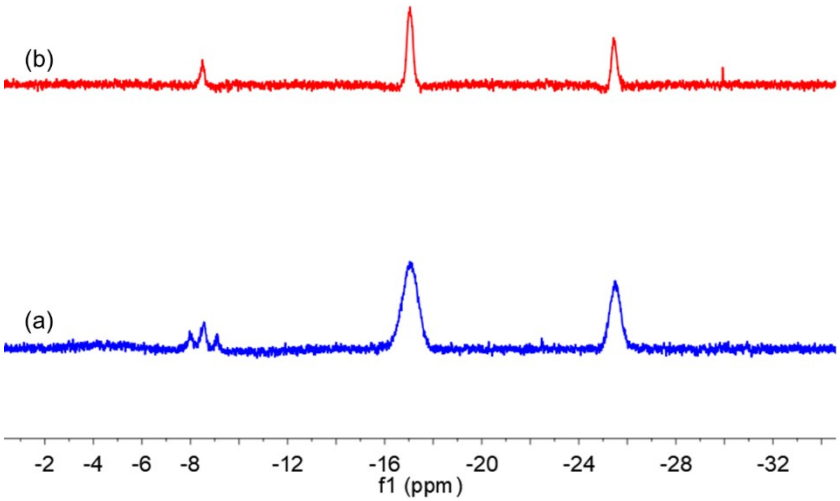

Fig. S5 The ^{11}B NMR (a) and $^{11}B\{^{1}H\}$ NMR (b) spectra of $K[B_3H_7NH_2BH_2NH_2B_3H_7]$ in CD_3CN, which was isolated from the reaction of $K[NH_2BH_3]$ with $NH_3B_3H_7$.

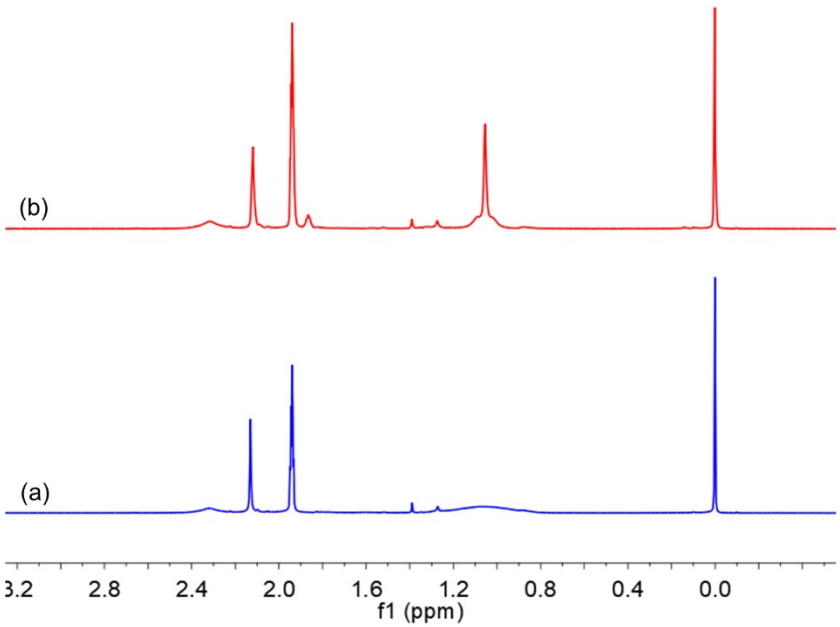

Fig. S6 The ^{1}H NMR (a) and $^{1}H\{^{11}B\}$ NMR (b) spectra of $K[B_3H_7NH_2BH_2NH_2B_3H_7]$ in CD_3CN, which was isolated from the reaction of $K[NH_2BH_3]$ with $NH_3B_3H_7$.

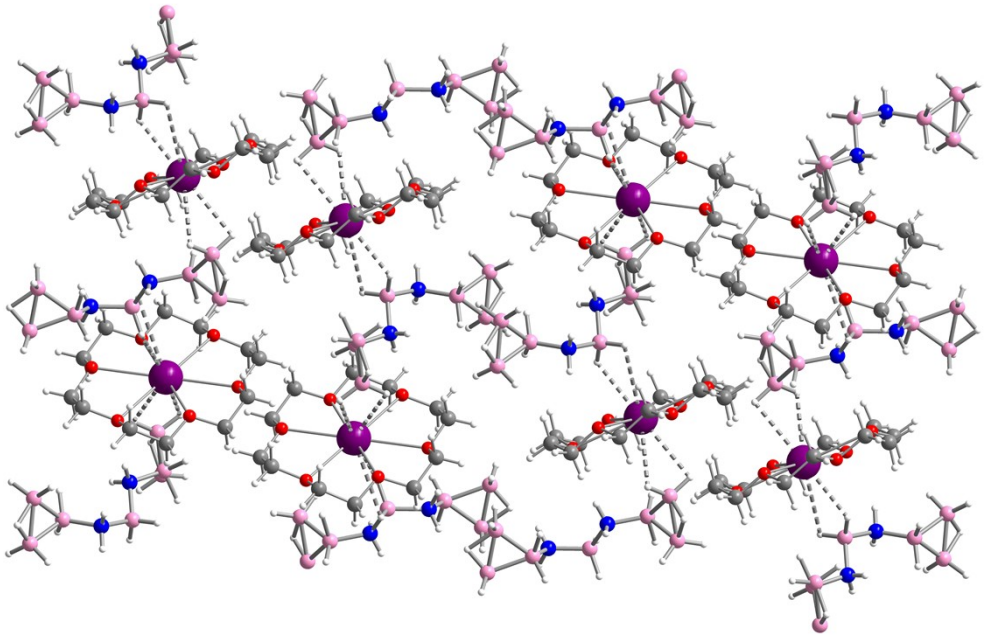

Fig. S7 Single-crystal structure of $K[B_3H_7NH_2BH_2NH_2B_3H_7]\cdot$18-crown-6 adduct. Colors: N, blue; B, pink; O, red; H, white; C, gray; K, purple.

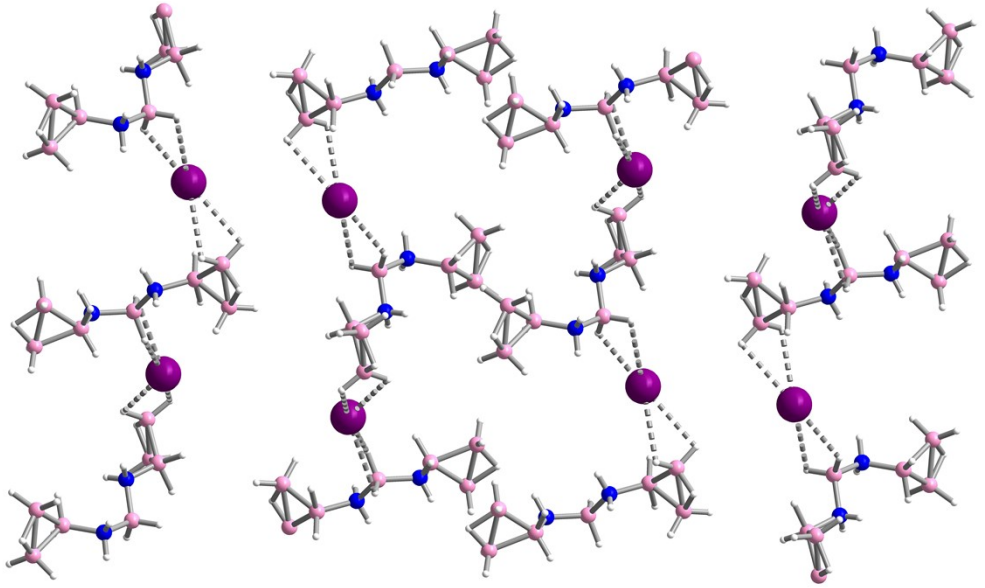

Fig. S8 Single-crystal structure of the $K[B_3H_7NH_2BH_2NH_2B_3H_7]$ fragment of $K[B_3H_7NH_2BH_2NH_2B_3H_7]\cdot$18-crown-6 adduct. Colors: N, blue; B, pink; H, white; K, purple.

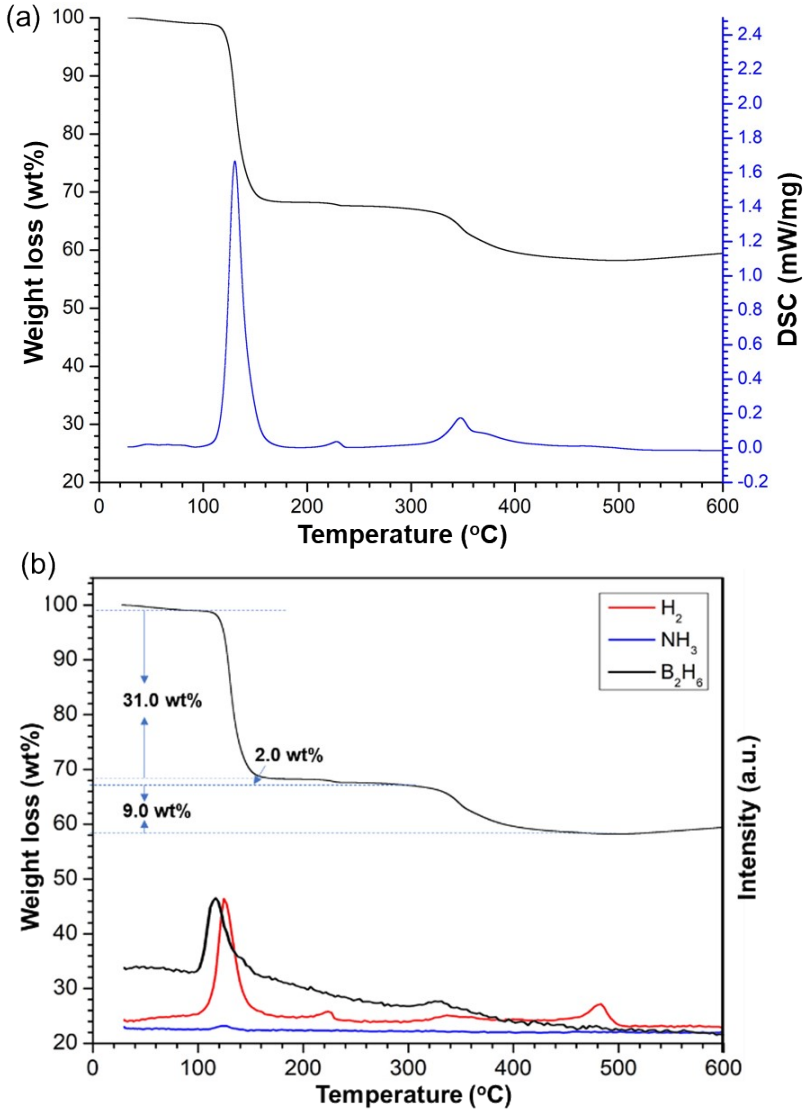

Fig. S9 The TGA-DSC (a) and TGA-MS (b) spectra of the prepared $K[B_3H_7NH_2BH_2NH_2B_3H_7]$ (5 °C/min, N_2).

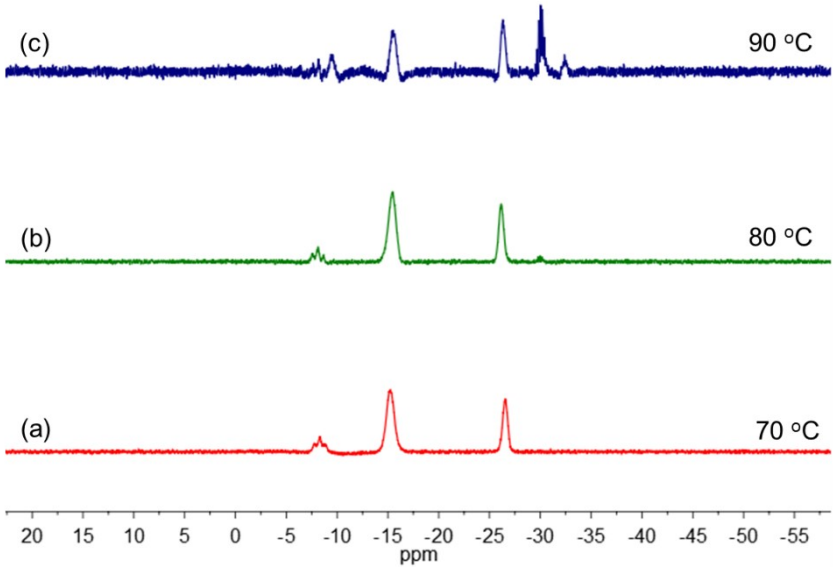

Fig. S10 ^{11}B NMR spectra of $K[B_3H_7NH_2BH_2NH_2B_3H_7]$ recorded after heating to a given temperature.

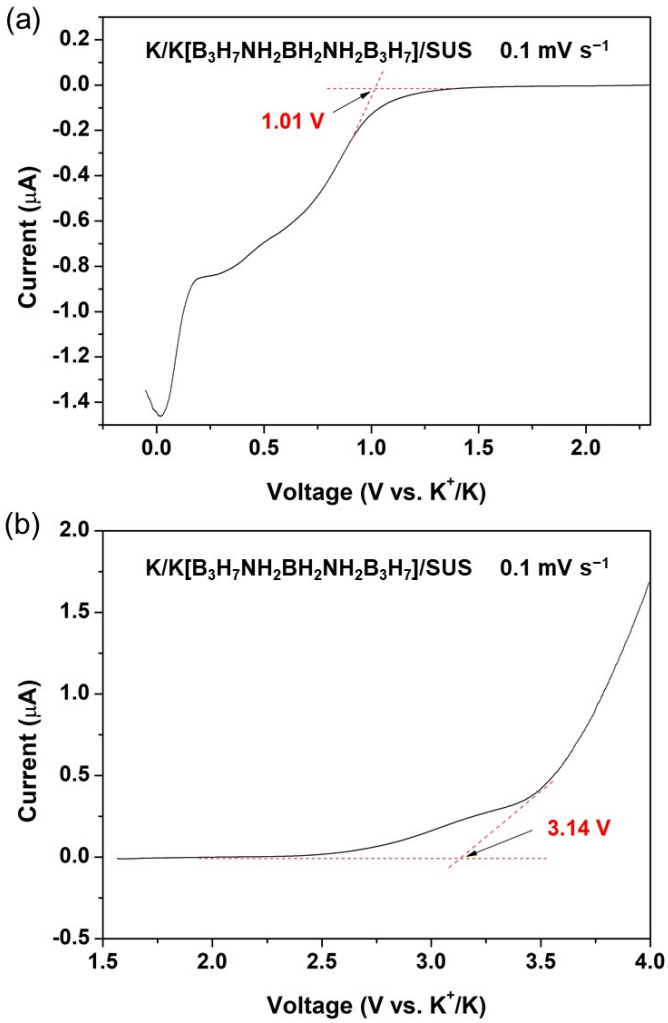

Fig. S11 LSV curves of $K[B_3H_7NH_2BH_2NH_2B_3H_7]$ SSE at scan ranges of OCV to −0.05 V (K^+/K) (a) and OCV to 4.0 V (K^+/K) (b).

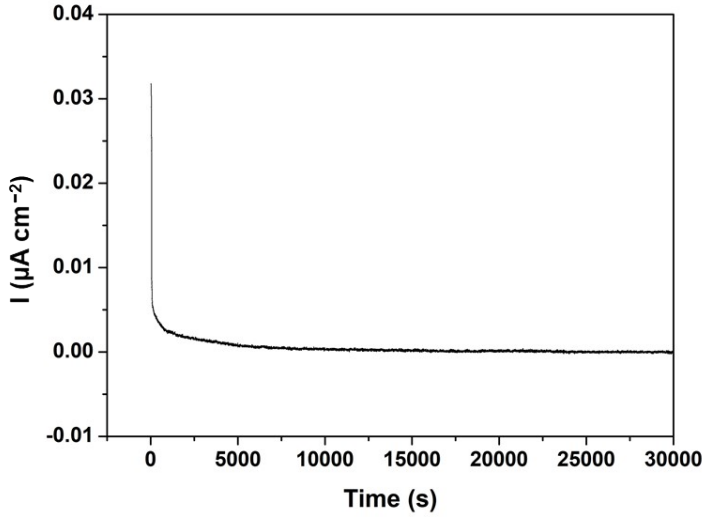

Fig. S12 DC polarization curve of a SUS/$K[B_3H_7NH_2BH_2NH_2B_3H_7]$/SUS cell.

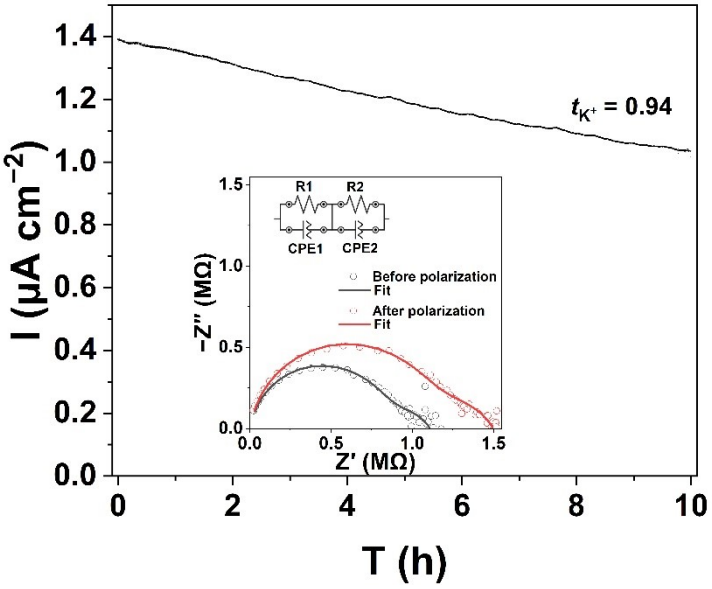

Fig. S13 DC polarization curve of a K/K[$B_3H_7NH_2BH_2NH_2B_3H_7$]/K cell. Inset is the EIS spectra of the cell before and after polarization.

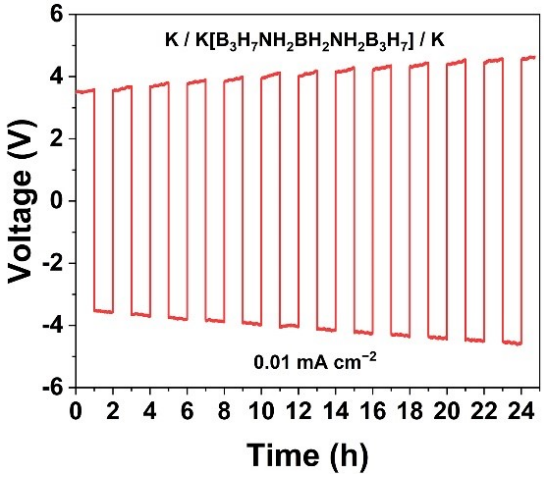

Fig. S14 Galvanostatic cycling of a K/K[$B_3H_7NH_2BH_2NH_2B_3H_7$]/K cell at a constant current density of 0.01 mA cm^{-2}. Temperature: 45 °C.

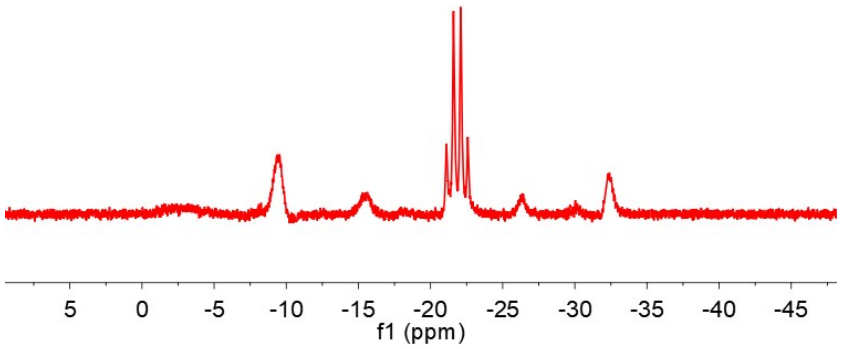

Fig. S15 The ^{11}B NMR spectrum of the reaction solution of $K[NH_2BH_3]$ with $NH_3B_3H_7$ in THF.

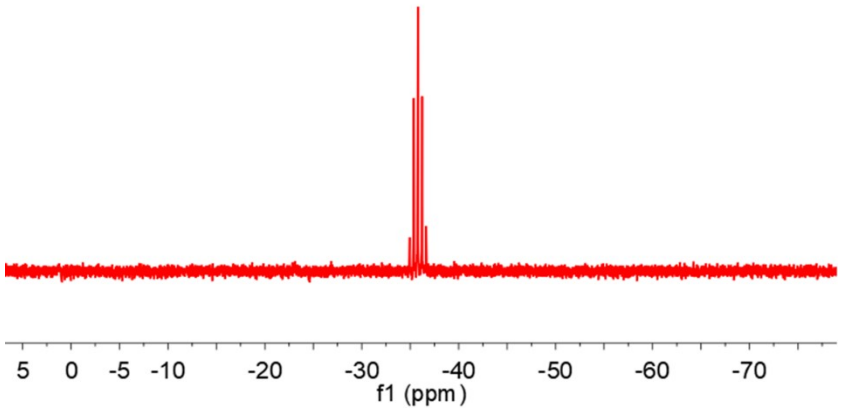

Fig. S16 The ^{11}B NMR spectrum of KBH_4 formed in the reaction of $K[NH_2BH_3]$ with $NH_3B_3H_7$ in DMSO.

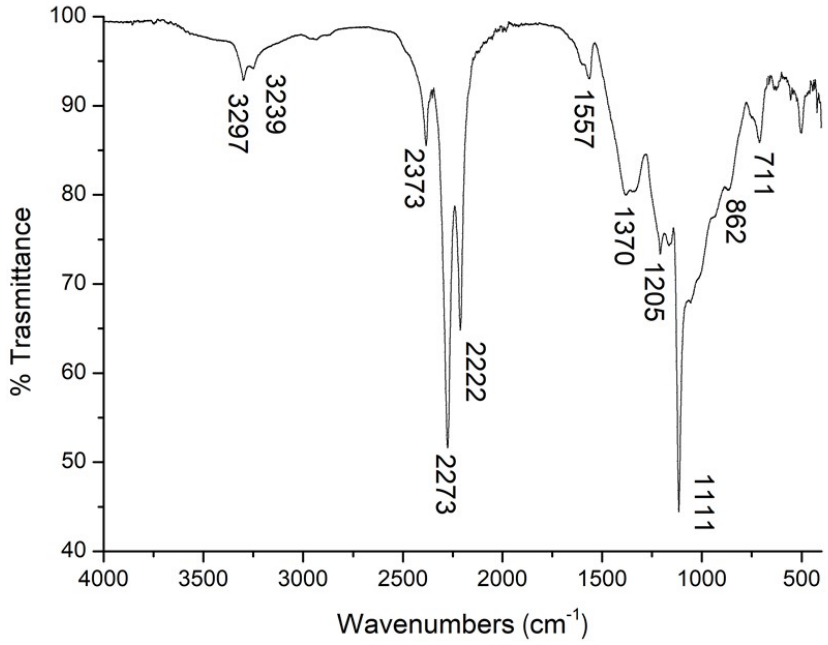

Fig. S17 The IR spectrum of $[NH_2BH_2]_n$ formed in the reaction of $K[NH_2BH_3]$ with $NH_3B_3H_7$.

3. Tables:

Table S1 Experimental and crystallographic details for $K[B_3H_7NH_2BH_2NH_2B_3H_7]$

Formula sum	$C_{24}H_{88}B_{14}K_2N_4O_{12}$
Formula weight	854.52
Wavelength	1.54184 Å
Crystal system	monoclinic
Space group	I2/c
Cell parameters	a = 16.5487(3) Å b = 9.1479(2) Å c = 34.5522(7) Å β = 95.294(2)°
Cell volume	5208.40(18) $Å^3$
Z	4
Calc. density	1.090 g/cm^3
Absorption coefficient	1.992 mm^{-1}
F (000)	1856.0
Crystal size	0.02×0.02×0.02 mm^3
Theta range for data collection	10.006 to 142.996°
Index ranges	-20≤h≤20, -7≤k≤11, -41≤l≤42
Reflections collected	10316
Independent reflections	4924 [R(int)= 0.0573, R(sigma)= 0.0662]
Data/restraints/parameters	4924/1/341
Goodness-of-fit on F^2	1.079
Final R indexes [I>=2σ (I)]	R_1= 0.0577, wR_2= 0.1484
Final R indexes [all data]	R_1= 0.0755, wR_2= 0.1581
Measured temperature	149.99(10) K
Largest diff. peak and hole	0.53 and -0.56 e/ $Å^3$

Table S2 Selected bond distances (Å) for crystal structure

Distances (Å)			
B5-B7	1.827(4)	O2-C2	1.419(4)
B5-B6	1.796(4)	O2-C3	1.424(3)
B3-B2	1.751(4)	C5-C6	1.498(5)
B3-B1	1.814(4)	C7-C8	1.499(4)
B7-B6	1.732(4)	C9-C10	1.486(4)
B2-B1	1.764(4)	C11-C12	1.490(4)
K1-B1	3.257(3)	C1-C2	1.493(4)
N2-B5	1.569(3)	C3-C4	1.482(5)
N2-B4	1.579(3)	O4-C6	1.414(3)
N1-B4	1.577(3)	O4-C7	1.419(3)
N1-B3	1.573(3)	O1-C12	1.425(3)
O3-C5	1.418(3)	O1-C1	1.420(3)
O3-C4	1.427(3)	K1-O1	2.7634(17)
O5-C8	1.427(3)	K1-O3	2.8043(17)
O5-C9	1.426(3)	K1-O5	2.8403(15)
O6-C10	1.423(3)	K1-O6	2.8666(15)
O6-C11	1.425(3)	K1-O2	2.7870(16)
K1-O4	2.8247(17)		

4. References:

1 X.-M. Chen, Y. Jing, J.-X. Kang, Y. Wang, Y. Guo and X. Chen, *Inorg. Chem*., 2021, **60**, 18466−18472.

2 H. V. K. Diyabalanage, T. Nakagawa, R. P. Shrestha, T. A. Semelsberger, B. L. Davis, B. Scott, A. K. Burrell, W. I. F. David, K. R. Ryan, M. O. Jones and P. P. Edwards, *J. Am. Chem. Soc*., 2010, **132**, 11836−11837.

3 M. J. Frisch, G. W. Trucks, H. B. Schlegel, G. E. Scuseria, M. A. Robb, J. R. Cheeseman, G. Scalmani, V. Barone, G. A. Petersson, H. Nakatsuji, X. Li, M. Caricato, A. V. Marenich, J. Bloino, B. G. Janesko, R. Gomperts, B. Mennucci, H. P. Hratchian, J. V. Ortiz, A. F. Izmaylov, J. L. Sonnenberg, D. Williams-Young, F. Ding, F. Lipparini, F. Egidi, J. Goings, B. Peng, A. Petrone, T. Henderson, D. Ranasinghe, V. G. Zakrzewski, J. Gao, N. Rega, G. Zheng, W. Liang, M. Hada, M. Ehara, K. Toyota, R. Fukuda, J. Hasegawa, M. Ishida, T. Nakajima, Y. Honda, O. Kitao, H. Nakai, T. Vreven, K. Throssell, Jr. J. A. Montgomery, J. E. Peralta, F. Ogliaro, M. J. Bearpark, J. J. Heyd, E. N. Brothers, K. N. Kudin, V. N. Staroverov, T. A. Keith, R. Kobayashi, J. Normand, K. Raghavachari, A. P. Rendell, J. C. Burant, S. S. Iyengar, J. Tomasi, M. Cossi, J. M. Millam, M. Klene, C. Adamo, R. Cammi, J. W. Ochterski, R. L. Martin, K. Morokuma, O. Farkas, J. B. Foresman and D. J. Fox, Gaussian 09, Revision D.01, Gaussian, Inc., Wallingford CT, 2016.

4 (a) T. Lu, F. Chen, *J. comput. Chem*., 2012, **33**, 580−592; (b) J. Zhang, T. Lu, *Phys. Chem. Chem. Phys*., 2021, **23**, 20323−20328.

5 W. Humphrey, A. Dalke and K. Schulten, *J. Mol. Graph*., 1996, **14**, 33−38.